Sens. & Instrumen. Food Qual. (2009) 3:70–80
DOI 10.1007/s11694-008-9067-8

ORIGINAL PAPER

Machine vision system for online inspection of freshly slaughtered chickens

Chun-Chieh Yang · Kuanglin Chao · Moon S. Kim

Received: 23 September 2008 / Accepted: 5 December 2008 / Published online: 24 December 2008

Abstract A machine vision system was developed and evaluated for the automation of online inspection to differentiate freshly slaughtered wholesome chickens from systemically diseased chickens. The system consisted of an electron-multiplying charge-coupled-device (EMCCD) camera used with an imaging spectrograph and controlled by a computer to obtain line-scan images quickly on a chicken processing line of a commercial poultry plant. The system scanned chicken carcasses on an eviscerating line operating at a speed of 140 chickens per minute. An algorithm was implemented in the system to automatically recognize individual carcasses entering and exiting the field of view, to locate the region of interest (ROI) of each chicken, to extract useful spectra from the ROI as inputs to the differentiation method, and to determine the condition for each carcass as being wholesome or systemically diseased. The system can acquire either hyperspectral or multispectral images without any cross-system calibration. The essential spectral features were selected from hyperspectral images of chicken samples. The differentiation of chickens on the processing line was then carried out using multispectral imaging. The high accuracy obtained from the evaluation results showed that the machine vision system can be applied successfully to automatic online inspection for chicken processing.

Keywords Multispectral images · Hyperspectral images · Line scan · Food safety · Poultry inspection

Introduction

American chicken plants process over eight billion birds annually. Processing plants seeking to satisfy increasing consumer demand by increasing output through faster processing are limited by the current inspection system, which limits each human inspector to examining a maximum of 35 birds per minute (bpm) on the processing lines. The Food Safety and Inspection Service (FSIS) of the United States Department of Agriculture (USDA) has implemented the Hazard Analysis and Critical Control Point (HACCP) program in processing plants throughout the country and has also been testing the HACCP-based Inspection Models Project (HIMP) [1]. This project includes a zero tolerance standard for chickens with infectious condition such as septicemia and toxemia, which must be removed from the processing line. Systemically diseased chickens show external symptoms of septicemia or toxemia. Septicemia is caused by the presence of pathogenic microorganisms or their toxins in the bloodstream, and toxemia is the result of toxins produced from cells at a localized infection or from the growth of microorganisms.

For poultry plants to meet government food safety regulations while maintaining their competitiveness to satisfy consumer demand, the development of new inspection technologies, such as automated computer imaging inspection systems, should be considered [2]. One possible solution to this challenge is for poultry processing plants to install online instrumental inspection systems that can accurately screen out unwholesome carcasses. Only questionable carcasses in the rejection line would then require

Mention of trade names or commercial products is solely for the purpose of providing specific information and does not imply endorsement or recommendation by the USDA.

C.-C. Yang · K. Chao (✉) · M. S. Kim
Food Safety Laboratory, USDA-ARS, Beltsville, MD 20705, USA
e-mail: kevin.chao@ars.usda.gov

"re-inspection" to ensure that wholesome carcasses are not discarded. This approach would dramatically reduce the number of birds requiring human inspection. An obvious benefit of automatic poultry inspection would be improved overall production efficiency of the processing plants.

There have been several research studies using multispectral imaging systems for chicken carcass inspection [3, 4]. Multispectral images contain spectral and spatial information from the surface of chicken carcasses, which both studies identified as being essential for efficient identification of contamination and systemic disease. Many studies [3–5] have shown that the proper selection of wavelengths is essential for successful multispectral imaging applications. Once specific wavelengths and image features that can increase classification accuracy for chicken inspection have been determined using data from a hyperspectral imaging system, it is usually necessary to implement them into a separate multispectral imaging system in order to achieve fast imaging for online inspection applications. Furthermore, considerable effort is required to ensure that a multispectral imaging system with significantly different hardware and software components can obtain the same results as the hyperspectral imaging system. Thus, a major challenge is the difficulty of cross-system calibration for implementing configurations and features to a multispectral imaging system [6].

More recent studies have used hyperspectral/multispectral line-scan imaging systems to overcome the challenges of cross-system calibration [4, 5]. Line-scan imaging systems were initially used for surface analysis studies. Images collected using hyperspectral line-scan imaging systems have been used for applications such as surface roughness measurement [7], rapid acquisition of fluorescence lifetime imaging [8], and prediction of nitrogen and phosphorus content in spring barley [9]. From these studies, hyperspectral line-scan imaging systems appear to be well suited for detecting differences in surface reflectance between wholesome and systemically diseased chickens.

For online inspection of poultry carcasses, line-scan machine vision systems should, ideally, be able to easily implement the multispectral image features and processing algorithms determined through hyperspectral imaging analysis, with minimal software adaptations and without the need for cross-system calibration. Therefore, in this research, a hyperspectral/multispectral line-scan automatic machine vision system for differentiation of wholesome and systemically diseased chickens was successfully developed. The system acquired hyperspectral line-scan images to determine the key wavelengths, region of interest, and input features for chicken differentiation. When switched over to acquire multispectral line-scan images, the same system was able to automatically sense the coming and leaving of a chicken carcass, locate the region of interest, and differentiate systemically diseased chickens from wholesome ones. Hyperspectral and multispectral imaging conducted on a commercial chicken processing line was used for the development and evaluation of this system, to ensure that the system can function appropriately for the needs of the poultry industry.

Materials and methods

System development and online evaluation

The machine vision system was developed and evaluated on a chicken eviscerating line at a Tyson Foods chicken processing plant (Cumming, GA, USA) in 2007. The line speed was 140 bpm. First, the system acquired sample images of 190 wholesome and seven systemically diseased chickens, for use in determining the region of interest, selecting the key wavebands, and obtaining the parameters for the differentiation algorithm. These images were acquired with the machine vision system in hyperspectral imaging mode, and the chicken conditions were determined by a USDA-FSIS veterinarian observing the birds on the processing line as they approached the machine vision system. Next, the system was switched to multispectral imaging mode, and online imaging was conducted to evaluate the differentiation algorithm and to determine the decision threshold, again based on the bird assessments by the veterinarian standing beside the system to observe the chickens on the processing line. Last, the system was run continuously in multispectral imaging mode for two 8-h shifts and its differentiation results were compared with the wholesome and systemically diseased bird counts produced by from the processing plant's inspectors who worked during those two shifts.

Line-scan machine vision system

The line-scan machine vision system consisted of an electron-multiplying charge-coupled-device (EMCCD) camera, an imaging spectrograph, an optical lens, two pairs of light-emitting-diode (LED) line lights, a controlling PC, and a power backup battery. Figure 1 showed the general scheme for the line-scan machine vision system. The instruments were assembled on a wheeled cart for convenient movement, easy access and operation, and flexible installment in the limited space of a poultry processing plant. The imaging part of the system, including the camera, the spectrograph, and the lens, was assembled to sit in the imaging platform. The cart was always positioned to provide for a distance of 914 mm between the shackle line and the lens. The lighting part of the system had two pairs

of line lights, an outer pair and an inner pair. One outer light and one inner light were mounted together on a single pivot joint to the right of the field of view, and the remaining two lights were mounted similarly on another pivot joint to the left of the field of view, such that on each side, the angles of illumination of the inner light and outer light were not independently adjustable. The joints were separated by 115 mm, each at a distance of 254 mm from the shackle line. The outer pair was positioned slightly ahead the inner pair, rather than with their forward faces flush, which allowed for some forward movement of the target surface within 25 mm of the shackle line so that the convex surface of a bird pushed slightly more forward than normal would still be adequately and uniformly illuminated. Since each light was composed of a vertical series of LED heads, the inner pair was positioned a half head higher than the outer pair to prevent interference between the two pairs. The pivot joints were fixed on one end of the lighting beam, which was mounted on slide blocks under the imaging platform so that the lights could be easily positioned, by forward/backward adjustment, at the appropriate distance from the shackle line. Three posts were installed on the cart to support the imaging and lighting parts. Slide blocks on the support posts also allowed the elevation of the imaging platform to be easily adjusted to the appropriate height for imaging. Another post supported the weight of the lighting beam. An acrylic panel mounted on the support posts shielded the camera hardware from dripping water overhead; panels of construction-grade plastic sheeting shielded the camera and computer hardware from excess water spray and splash of chicken carcass fluids in the processing environment. The plastic panels were fastened to the cart frame and overhead acrylic panel using adhesive-backed Velcro, allowing researchers to access the instruments as needed during system operation.

A PhotonMAX 512b EMCCD camera (Princeton Instruments, Roper Scientific, Inc., Trenton, NJ, USA), operating with a 10 MHz, 16-bit digitizer, was used to acquire images. Unlike a conventional CCD camera, the EMCCD camera can function with high multiplication gain to compensate for low illumination levels due to short exposure times. Thus, this camera was used for low-light, high-speed image visualization, which is essential for automatic online chicken inspection. While taking line-scan images, the camera was set for a 0.1 ms exposure time and an absolute multiplication gain of 45. An ImSpector V10 OEM imaging spectrograph (Spectral Imaging Ltd., Oulu, Finland) was used to produce spectral images from a linear field of view. A slit in front of the spectrograph collimates light for the pixels of the line-scan image being acquired, and the white light from each pixel is dispersed into contiguous wavelengths across the detector array by the spectrograph's prism/grating/prism system. Thus, when acquiring a line-scan image from the linear field of view, the machine vision system could simultaneously acquire spectral data for each pixel in the line-scan image. A Rainbow S6X11 C-mount lens (Schneider Optics, Inc., Hauppauge NY, USA) was used because its optimal spectral range of 400–1000 nm encompassed the spectral wavebands essential to effective poultry wholesomeness inspection. Four LL6212-WHI line lights (Advanced Illumination, Inc., Rochester, VT, USA) were used for their high-power broad-spectrum illumination, long lifetime, and lower level heat production. The current for these lights was set at 100 mA for each of the four channels, blue, green, red, and infrared, to obtain white light. The program to control the machine vision system and execute the

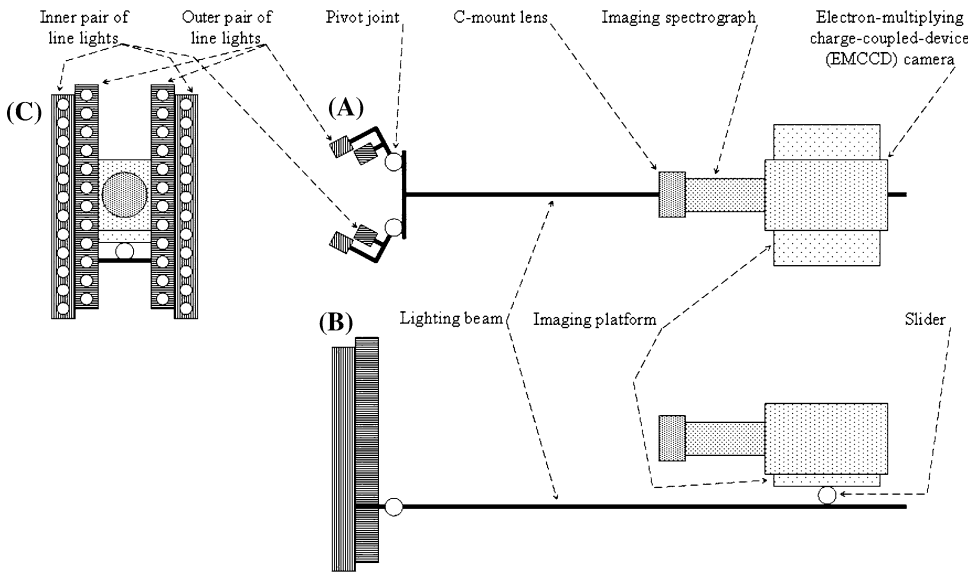

Fig. 1 The line-scan machine vision system in (A) overhead view, (B) side view, and (C) front view

differentiation algorithm was developed and operated on a LabVIEW 8.2 (National Instruments, Austin, TX, USA) platform.

Image acquisition

Each hyperspectral line-scan image acquired by the camera consisted of 512 × 512 pixels. For the 512 rows of pixels, the measurements contained within any single row comprised the reflectance value at one spectral waveband for the 512 spatial pixel coordinates of the line-scan image. For the 512 columns of pixels, the measurements contained within any one column comprised the 512-point reflectance spectrum for one spatial pixel coordinate of the line-scan image. To increase image acquisition speed, the size of the image was reduced by binning the spectral pixels by four (accumulating the intensities of every four pixels along the spectral dimension as one pixel measurement) to produce a hyperspectral line-scan image size of 512 × 128 pixels. Because this process was carried out in the hardware of the camera, it reduced the number of pixels to be converted and digitized for the computer to process, thus increasing the imaging speed of the machine vision system. Empirically, it was found that the intensities from the first 19 and the last 54 spectral channels were too low to be useful, due to characteristics of the light source and lens. Discarding these 73 channels, the remaining 55 spectral channels were retained for image acquisition. Thus, the final hyperspectral line-scan image size was set at 512 × 55 pixels.

The machine vision system in this study was capable of functioning in two imaging modes, hyperspectral imaging and multispectral imaging, and could be easily switched between the two. For conventional development of machine vision systems, specific spectral parameters would be determined first using a hyperspectral imaging system and then implemented in separate multispectral imaging system. The conversion and implementation of parameters from one system to the other usually involves time-consuming cross-system calibration. The capacity of a single system to operate in either hyperspectral or multispectral imaging mode can eliminate the need for cross-system calibration and ensure accurate performance. In the hyperspectral imaging mode, the machine vision system in this study acquired a 55-band spectrum for each of the 512 spatial pixels in every hyperspectral line-scan image, as described as above. For the multispectral imaging mode, specific individual wavebands were selected and only the reflectance measurements for these selected wavebands were digitized for the computer to process, while the rest were discarded by the hardware of the camera. Thus, there remained 512 pixels in the spatial dimension of the image but the pixels in the spectral dimension were further reduced from 55, enabling the system to operate even faster in multispectral imaging mode than was possible in hyperspectral imaging mode. For the development of this multispectral imaging system, hyperspectral image analysis was performed specifically to select specific wavebands to implement for the differentiation of wholesome and systemically diseased chickens by the same system operating in multispectral imaging mode.

The ability of the machine vision system's EMCCD camera to use a very short exposure time with a high gain setting and to select a limited number of pixels in the spectral dimension of the multispectral line-scan images were vital to the system's successful operation in multispectral imaging mode for differentiating wholesome and systemically diseased chickens. These factors enabled the system to effectively image birds on a high-speed processing line that operated at a speed of 140 carcasses per minute.

System calibration and image correction

Before any period of continuous poultry imaging (such as an 8-h shift on a chicken processing line), the machine vision system must be calibrated in five steps to ensure accurate performance. In the first step, focusing the lens, a grid paper was presented as a focal target at a distance of 914 mm from the front of the lens, equal to the expected distance from the lens to the poultry carcass surface. The grid also served as a reference measure for adjusting the field of view, to translate a vertical length of 178 mm in the illuminated imaging area into the 512 spatial pixels. Translating 178 mm linear field of view into 512 spatial pixels, each pixel covered an area of 0.348 × 0.348 mm^2.

In the second step, optimizing the illumination, a white Spectralon 99% diffuse reflectance target (Labsphere, Inc., North Sutton, NH, USA) was presented at the 914 mm distance in front of the lens. The angles of the pivot joints (to which the line lights were mounted) were adjusted to obtain the maximized reflectance intensity of the line-scan images. The outer pair of line lights was positioned slightly ahead of the inner pair to overcome the challenge presented by the curved poultry surfaces and the expected variation in the surface presentation distance from the camera lens (within 25 mm of the 914 mm distance). Regardless of the convex surface of a bird, its surface would be adequately and uniformly illuminated for line-scan imaging.

In the third step, aligning the spectrograph, a mercury-neon pencil light was used with the LED line lights turned off. The lamp of the pencil light contains mercury to dominate the output spectrum, and also contains neon as a starter gas. Thus, the spectral output of the pencil light in the first minute of usage is that of neon, and afterwards turns to that of mercury. The spectrograph must be physically aligned for uniform waveband dispersal across the

spectral dimension for each spatial pixel. This alignment was ascertained by examining the spectral dispersal of the 55 wavebands for each of the 512 spatial pixels for a line-scan image: with proper alignment, the highest intensity value among all 55 wavebands will occur at the same spectral coordinate for each of the 512 spatial pixels. Within a single line-scan image, acquired using a neon-mercury calibration lamp to illuminate a white background, the specific spatial and spectral coordinates X and Y were found at (x,y) for the pixel with the highest intensity. Then, for the first spatial pixel in the line-scan image (i.e. all pixels for which spatial coordinate $X = 1$), the spectral intensity at spectral coordinates $y - 1$, y, and $y + 1$ were compared to determine if the intensity at y was greater than both the intensities at $y - 1$ and $y + 1$. Similarly, for the 512th spatial pixel in the line-scan image (i.e. all pixels for which spatial coordinate $X = 512$), the spectral intensity at spectral coordinates $y - 1$, y, and $y + 1$ were compared to determine if the intensity at y was greater than both the intensities at $y - 1$ and $y + 1$. The waveband alignment of the spectrograph was correct if y was found to correspond to the local spectral maxima for both the first pixel and the 512th pixels.

In the fourth step, correlating the spectral channels to wavebands, the raw spectra for the mercury-neon pencil light were used again. There are six peaks of the spectra corresponding to known reference wavelengths: 436 and 546 nm from mercury light, and 614, 640, 703, and 724 nm from neon light. These wavelengths were assigned to the wavebands corresponding to six apparent peaks (Fig. 2). After obtaining a 55-waveband spectrum, the second-order polynomial regression, in which λ is the wavelength (nm) and scn is the spectral channel number, was calculated based on the six known wavelength peaks of the mercury and neon spectra (Fig. 2), to calibrate the spectral dimension. Function 1 was obtained to correlate channels to wavebands as follows:

$$\lambda = -0.001 \times scn^2 + 6.642 \times scn + 382.451 \quad (1)$$

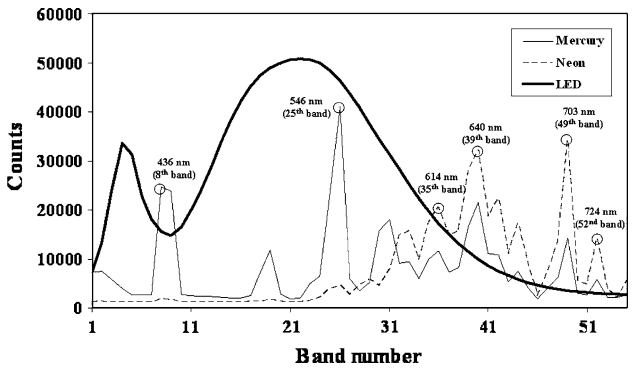

Fig. 2 The spectra for mercury pencil light, neon pencil light, and light-emitting-diode (LED) light

Function 1 showed the relationship between spectral channels and wavebands in the range from 389 (the first channel) to 744 nm (the 55th channel), with an average bandwidth of 6.57 nm. The correlation coefficient of the linear regression between calibrated and expected wavelengths was 0.999. The coefficient closing to one indicated the accurate calibration and linear relationship among the range of known reference wavelengths.

In the fifth step, preparing flat-field correcting images, some line-scan images of a Spectralon diffuse reflectance target were acquired. They were averaged to obtain a white reference image, W. Then, the lens was completely covered and some dark current images were acquired and averaged to obtain a dark reference image, D. This step, of preparing white and dark reference images, was repeated whenever the machine vision system was switched from hyperspectral imaging mode to multispectral imaging mode, since the image size would be different. For each raw line-scan image I_0, the pixel-based flat field correction was performed to obtain the corrected line-scan image I as follows:

$$I = \frac{I_0 - D}{W - D} \quad (2)$$

The relative intensity of the corrected image was used for image processing and classification afterward.

After obtaining the corrected relatively intensity image, image segmentation was performed by masking to separate the poultry carcass from the image background. A black matte-surface acrylic panel hung behind the chickens on the processing line provided the background for imaging. Because the highest intensity differences between chicken carcass pixels and background pixels were empirically observed to occur at the 620 nm waveband, the reflectance intensity at 620 nm was used for image segmentation to separate chicken from background. The pixels in which the relative intensity at 620 nm was lower than the threshold 0.1 would be treated as black background and discarded. Pixels for which the relative intensity at 620 nm was lower than the threshold value of 0.1 were treated as background pixels and discarded – i.e. omitted from further processing for carcass differentiation. Only non-background pixels were used for carcass differentiation. The threshold value of 0.1 was determined by trial and error.

Poultry carcass detection and region of interest location

After the machine vision system was calibrated, online imaging of chicken carcasses was begun. For carcass differentiation, full wingtip-to-wingtip scanning of each bird was not necessary. Moreover, the wings of adjacent birds always overlapped each other on the processing line, so wingtip-to-wingtip line-scan imaging was rendered

unfeasible without major modification of the processing line configuration. A method was developed to automatically detect the entry of each chicken carcass into, and its exit from, the camera's field of view. As the camera acquired each new line-scan image, the relative reflectance at the 620 nm waveband was examined for each pixel within the upper part of the line-scan image, termed the 'carcass detection length,' which consisted of 200 pixels in this case. The initial entry of the carcass into the field of view was recognized when the relative reflectance at the 620 nm waveband increased over the threshold value of 0.1 for any single pixel within these uppermost 200 pixels, which corresponded to the entry of the leading edge of the leg of a carcass properly hung on a processing line shackle shackle. This method only examines the uppermost 200 pixels of each line-scan image in order to disregard possible anomalies in the position of the wings or any eviscerated organs as the carcass comes into view. After the detection of the first line-scan image containing an over-threshold pixel within the carcass detection length, subsequent line-scans were monitored as the chicken continued to move across the field of view and additional pixels, located below the first detected over-threshold pixel and above the 200th pixel, began showing increased relative reflectance values at 620 nm. As the line-scans continued, the indices of pixels whose reflectance values had not yet crossed over the threshold value were noted until, ultimately, a line-scan was found that contained only one pixel (or several adjacent pixels) remaining below the first detected pixel and above the 200th pixel for which the reflectance value was still below 0.1. When the reflectance value crossed the threshold value for that last pixel in the next line-scan image, then the location of that pixel *P* was identified as the point on the leading edge of the chicken image corresponding to the junction of the thigh and the side of the abdomen. The point *P* was designated as the start point (SP), and the line-scan image containing this point was the starting line (SL), for the individual carcass currently being scanned.

After identifying the SL, subsequent line-scan images were acquired and the ending line (EL) was identified when the reflectance value at the pixel location corresponding to the SP crossed the threshold value from above to below, indicating that the main body of the bird had already passed through the field of view. The reflectance intensities at 620 nm from wing and thigh areas were lower than those from other areas because of shadows and irregular surfaces [4]. Eliminating the wing and thigh areas from consideration would increase the differentiation accuracy that can be achieved. Thus, only the carcass surface scanned between SL and EL and below SP would be considered further to locate the region of interest (ROI) for each carcass. Because the achievable differentiation accuracy could be increased by eliminating the wing and thigh areas from consideration, the potential region of interest (ROI) to be used for classifying each carcass was only evaluated using pixels located below the SP coordinate in the line-scan images between the SL and EL for each bird.

The location of each potential ROI to be evaluated for use in differentiating carcasses was defined by the top boundary, TB, and the bottom boundary, BB, each of which specifies a percentage of the pixels within the line-scan image, as counted from the SP vertical coordinate down to the lowermost non-background pixel. For each scanned line between the SL and EL, the ROI consists only of pixels between TB and BB. Only the pixels in the ROI, from SL to EL and from TB to BB, were considered for poultry carcass differentiation (Fig. 3).

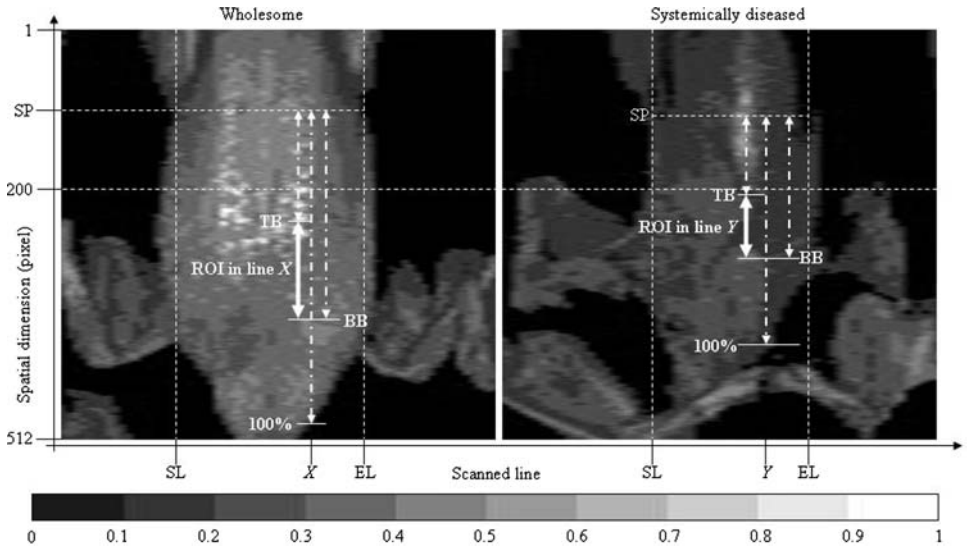

Fig. 3 The location for the region of interest (ROI)

Key waveband selection and poultry carcass differentiation

For each ROI considered, the spectral difference was calculated between the average spectrum of ROI pixels of wholesome birds and the average spectrum of ROI pixels of systemically diseased birds. The waveband for which the highest difference value occurred was selected as the key waveband WI. The average and standard deviation (SD) values for relative reflectance of wholesome and systemically diseased ROI pixels at waveband WI, obtained for the same sample chicken images, were used for single-band intensity-based differentiation of chicken carcasses.

For each ROI considered, the average spectrum of wholesome ROI pixels and the average spectrum of systemically diseased ROI pixels (calculated above) were examined to identify major peaks (local spectral maxima). The wavebands at which these peaks occurred were selected for consideration as the top waveband, WRT, for use in a two-waveband ratio for differentiating wholesome and systemically diseased chickens. Each of these peak wavebands was paired with a bottom waveband, WRB, corresponding to the nearest lower-waveband local spectral minimum. Ratio values were thus calculated as the WRT intensity divided by the WRB intensity for each waveband pair. The ratio values were calculated for all wholesome ROI pixels and all systemically diseased ROI pixels from the sample chicken images, and the average and standard deviation (SD) of the ratio values were used for ratio-based differentiation of chicken carcasses.

After the selected parameters for intensity and ratio differentiation were determined, a differentiation algorithm was developed. The algorithm contained two mapping functions, one defined for intensity differentiation and another for ratio differentiation. Each mapping function converted the input value, either a pixel's intensity at waveband WI or the ratio of a pixel's intensities at wavebands WRT and WRB, into an estimate of that pixel's possibility of indicating the systemically diseased condition. For each mapping function, the output value was assigned to be one when the input value, was equal to or less than the average value for systemically diseased chickens. The output value was assigned to be zero when the input value was equal to or greater than the (average − SD) value for wholesome chickens. For inputs between those values, the output value assignment decreased linearly from one to zero. A higher output value indicated a higher possibility for the image pixel to be an indicator of systemic disease. The primary reason for defining the mapping functions on the average systemically diseased values and the (average − SD) wholesome values was that wholesome ROI pixels tended to have higher values with less pixel-to-pixel variation both for intensity at waveband WI and for the intensity ratio using WRT and WRB, compared to systemically diseased ROI pixels. It was observed that pixels could be correctly classified whenever the input values occurred within the range of 97.5% confidence for wholesome chickens or in the range of 50% confidence for systemically diseased chickens.

After the SL was detected for an individual carcass, the mapping functions were applied to each ROI pixel in every line-scan image between the SL and EL, thus producing for each ROI pixel one output value for intensity-based differentiation and another for ratio-based differentiation. When the EL was detected, the outputs for all the ROI pixels were averaged to calculate the possibility of that carcass being systemically diseased. The average was compared against a decision threshold value that was calculated from applying the differentiation algorithm to the new images of wholesome and systemically diseased chickens acquired during multispectral online inspection. If a carcass's average output was higher than or equal to the decision threshold, the carcass was identified as systemically diseased.

Results and discussion

Figure 4 shows the range of the differences of the spectral intensities between wholesome and systemically diseased chickens that occurred for the ROIs defined by various values of TB and BB, the top and bottom ROI boundaries, respectively. For each ROI, the spectral difference range includes the spectral difference value at each of the 55 wavebands for which the system acquired data when in hyperspectral imaging mode. The results showed that the maximum spectral difference between the average spectrum of wholesome ROI pixels and the average spectrum of systemically diseased ROI pixels occurred for one of the 55 wavebands when the ROI was defined by TB of 40% and BB of 60%.

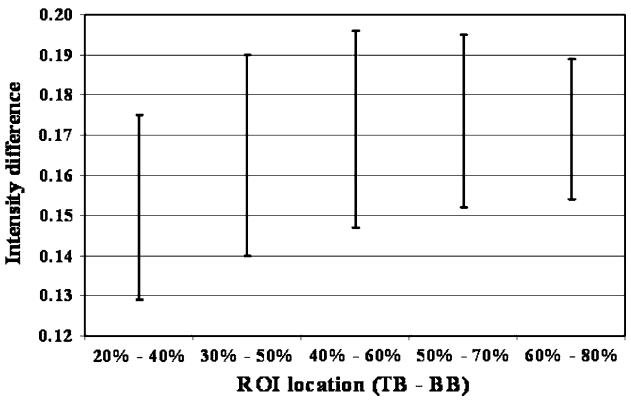

Fig. 4 For each of five different ROIs, the maximum and minimum values that occurred among the relative intensity difference values (between average wholesome and average systemically diseased ROI pixels) calculated for 55 wavebands

Figure 5 shows the average spectra for wholesome chicken pixels and systemically diseased pixels that were calculated for pixels in the 40–60% ROI in the sample chicken images. Three local maxima were identified in these spectra, occurring at 455, 534, and 620 nm. Each of these wavebands was paired with the nearest lower-wavelength waveband at which a local spectral minimum occurred: the 455, 534, and 620 nm peaks were thus paired with the 435, 495, and 580 nm valleys, respectively. The ratio of the reflectance intensities for each pair was evaluated for two-waveband ratio-based differentiation of wholesome and systemically diseased chickens. The value of the difference between average wholesome ratio and average systemically diseased ratio was calculated for each waveband pair and the results are shown in Table 1. The waveband pair of 580 and 620 nm produced the greatest difference between average ratio for wholesome ROI pixels and average ratio for systemically diseased ROI pixels, and thus were selected as the key wavebands WRB and WRT.

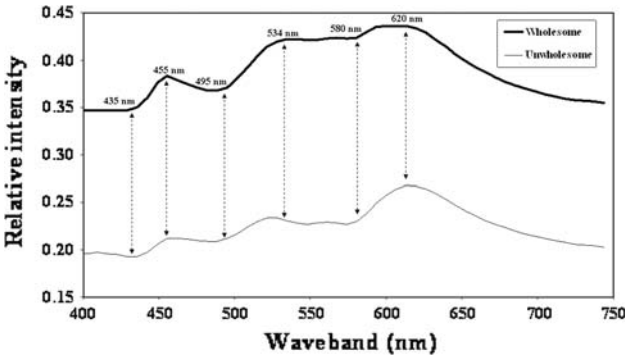

Fig. 5 The average ROI pixel spectra for wholesome chickens and the average ROI pixel spectral for systemically diseased chickens, used to select key wavebands for ratio-based differentiation

Table 1 The difference between average wholesome ratio and average systemically diseased ratio for each waveband pair selected for ratio differentiation

Waveband pair	Difference
435/455 nm	0.003
495/534 nm	0.039
580/620 nm	0.116

The average spectrum of wholesome ROI pixels and the average spectrum of systemically diseased ROI pixels, shown in Fig. 5, were used to calculate a difference spectrum that was analyzed for the selection of key waveband WI for single-band intensity-based differentiation. The spectral range between 567 and 580 nm showed the greatest difference values between the average wholesome and average systemically diseased spectra. To simplify the differentiation algorithm, the 580 nm waveband was selected for WI since it was already selected for WRB for two-band ratio-based differentiation. This selection, along with the selection of the 620 nm waveband as WRT (same band used for image segmentation to remove the image background), provided the benefit of minimizing the number of different wavebands needed for conducting multispectral inspection, thus potentially helping to minimize data processing time and maximize operation speed for the system. With only two wavebands needed to conduct differentiate wholesome and systemically diseased chicken images, the size of the line-scan images produced by the inspection system in multispectral imaging mode was 512 spatial pixels × 2 spectral pixels.

After selecting the key wavebands, the parameters for the mapping functions of the differentiation algorithm were determined by calculating the mean and standard deviation (SD) values of the intensities at the 580 nm and of the ratio of intensities between 580 and 620 nm from the ROI of the sample images of wholesome chickens and the sample images of the systemically diseased chickens. Figure 6 shows the results. The mean values for systemically diseased chickens and the (average − SD) values for wholesome chickens were used for the mapping functions. Applying the mapping function for intensity differentiation to each pixel in the ROI, the output value was equal to one when the input, the relative intensity at WI, was equal to or

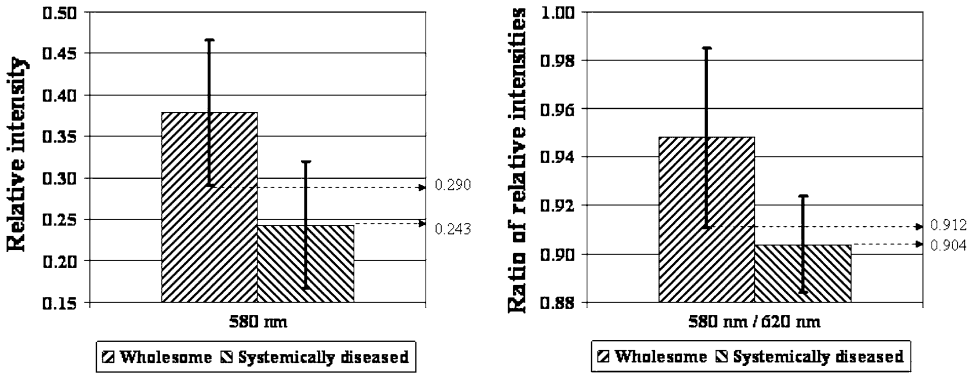

Fig. 6 The mean and standard deviation values for the relative intensity, and for the two-waveband ratio value for waveband pair 580 and 620 nm, of wholesome and systemically diseased ROI pixels

less than 0.243. The output value was equal to zero when the input was equal to or greater than 0.290. For input values in between, the output assignment decreased linearly from one to zero. Applying the mapping function for ratio differentiation to each pixel in the ROI, the output value was equal to one when the input, the ratio of the relative intensities at WRB and WRT, was equal to or less than 0.904. The output value was equal to zero when the input was equal to or greater than 0.912. For input values in between, the output value decreased linearly from one to zero. Each pixel in the ROI for a chicken carcass produced one output from the mapping function for intensity differentiation and another output from the mapping function for ratio differentiation. When line scanning reached the EL of a carcass, all of the outputs from both mapping functions were averaged to calculate the possibility of this carcass being systemically diseased.

After the algorithm was defined, the machine vision was run to inspect 63 systemically diseased chickens which were identified by a USDA-FSIS veterinarian online right before the location of the system. After the differentiation algorithm was defined, the machine vision system was run in multispectral imaging mode to inspect chickens for a period during which 63 systemically diseased chickens were identified on the processing line by a USDA-FSIS veterinarian observing the birds immediately before they entered the image system's field of view. The final decision output for each of these 63 birds was always higher than 0.65 and thus the decision threshold value was assigned: any carcass for which the final decision output was higher than or equal to 0.65 would be identified by the system as systemically diseased. Then, the machine vision system was run continuously in multispectral imaging mode for two 8-h shifts to inspect chicken carcasses on the processing line. The results of the system were compared to the bird counts produced by processing plant's inspectors during the same shift. It was noted that the machine vision system was installed after the beginning of the shift due to logistical issues; consequently, the number of chickens inspected by the machine vision system was lower than that inspected by the human inspectors. It was reasonably assumed that the systemically diseased chickens existed randomly in a normal distribution among all the processed chicken carcasses. Therefore, the rate of systemically diseased chickens over all carcasses inspected by the machine vision system could be compared to the one by the inspectors.

Figure 7 shows the results for online carcass inspection from the machine vision system in the first shift. During this shift, 45,456 poultry carcasses were inspected by the machine vision system. The machine vision system identified 177, or 0.39%, of the carcasses as systemically diseased chickens. During the same shift, the inspectors

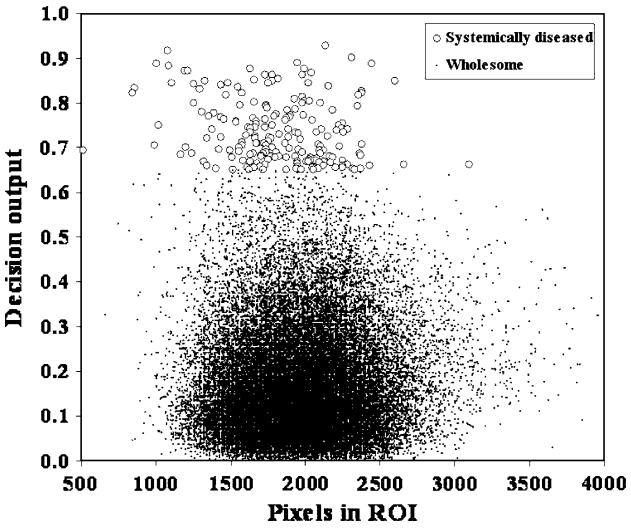

Fig. 7 The differentiation results of the machine vision inspection system for continuous multispectral inspection during the first 8-h processing shift

identified 84, or 0.16%, of the chickens as systemically diseased, among the 53,563 chickens in total that they inspected. The machine vision system identified more systemically diseased chickens than the inspectors. The primary reason for high misclassification of systemically diseased chickens may have been the intense steam from the high moisture environment clouding the lens, which would have reduced the overall reflectance from the carcasses that was detectable by the system. When the machine vision system was used for the imaging of individual carcasses with the assistance of the USDA-FSIS veterinarian for identifying bird condition, effort was taken by the researchers to clean the lens and take advantage of time periods in which the moisture was slightly less for optimal imaging. When the system was run unattended and continuously for eight hours, such efforts were much less due to exhaustion of human labor. It could explain why most of systemically diseased chickens identified by the machine vision system had the decision outputs in the range of 0.75 and 0.65, when the decision outputs of many wholesome chickens located in the range of 0.65 and 0.55. To improve the environmental condition, a large fan was installed, after the first shift ended, near the machine vision system to blow steam away from the system. The machine vision system was then run for another 8-h shift.

Figure 8 shows the inspection results from the second shift. The machine vision system scanned 61,020 chickens in total and identified 66, or 0.11%, of the chickens as systemically diseased. The inspectors observed 64,972 carcasses in total, and identified 71, or 0.11%, of them as systemically diseased. These results showed that the performance of the machine vision system was similar to that of the inspectors. In Fig. 8, the decision outputs for

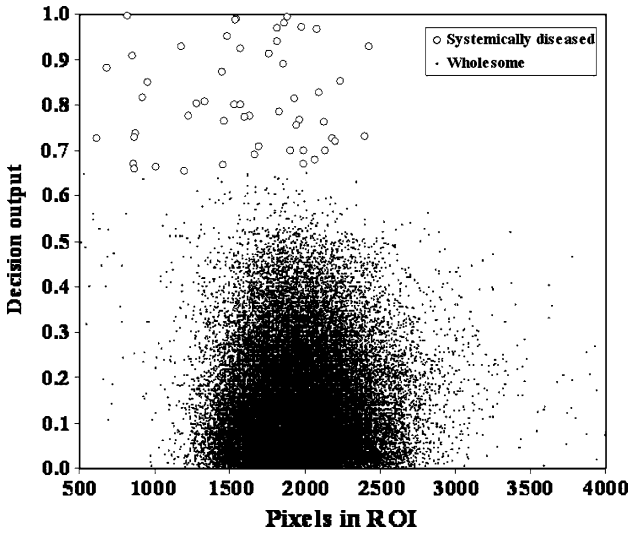

Fig. 8 The differentiation results of the machine vision system for continuous multispectral inspection during the second 8-h processing shift

systemically diseased chickens were distributed normally in the range between 0.65 and 1, and the decision outputs for wholesome chickens were distributed mainly in the range between 0 and 0.40. For the chickens whose decision outputs were higher than or equal to 0.65, the number of ROI pixels per bird was always less than 2,500. For the chickens whose decision outputs were lower than 0.65, the ROIs varied from 500 to 4,000 pixels. The clear separation between the wholesome birds and systemically diseased birds in Fig. 3, based on the 0.65 threshold value and ROI size, suggests that the machine vision system is capable of accurately differentiating wholesome and systemically diseased chicken carcasses, and that the 0.65 decision threshold is appropriately set for the differentiation algorithm.

Figures 7 and 8 show that chicken ROI size varied between 500 and 4,000 pixels, and that most ROIs occurred within the 1,500 to 2,800 pixel range. The normal distribution for ROI size indicated that the machine vision system was able to scan an adequate area of each carcass surface and quickly acquire data sufficient for representing the condition of the carcass. The differentiation results also suggest that the multispectral inspection algorithm was designed appropriately for rapidly retrieving line-scan image data from the high-speed EMCCD camera, locating the ROI pixels, and calculating the decision output for each bird, at an operation speed adequate for the 140 bpm processing line. The mapping functions of the differentiation algorithm were simple, which could benefit high speed algorithm execution, and produced highly accurate differentiation of carcasses. The results, particularly from the second shift in Fig. 8, demonstrated that the line-scan machine vision system was successfully developed and could be applied to the poultry processing lines to increase efficiency and reduce human error and labor.

It should noted that when the machine vision system is to be used for different populations of chickens, possibly varying in season, geography, or growth conditions, the procedure for collecting and analyzing sample images to locate the ROI, select key wavebands, and determine algorithm parameters should be repeated for each new population. The location of ROI might also vary if chickens are presented for imaging on a different processing line configuration, but the design of the machine vision system is flexible enough for adaptation to such challenges.

Conclusions

A line-scan machine vision system, consisting of an electron-multiplying charge-coupled-device (EMCCD) camera, an imaging spectrograph, and two pairs of light-emitting-diode (LED) line lights, was developed for online differentiation of systemically diseased chickens from wholesome chickens on a high speed commercial processing line. The system could be easily switched to operate in either hyperspectral imaging mode or multispectral imaging mode. A method was developed to detect the entry of a chicken carcass into, and its exit from, the camera field of view. The region of interest (ROI) for a carcass was defined as the area between 40% and 60% of the length from the start point (SP) vertical coordinate to the bottommost non-background pixel in each line-scan image between the start line (SL) and the end line (EL). The waveband of 580 nm was selected for intensity differentiation and ratio differentiation. The waveband of 620 nm was selected for image segmentation and ratio differentiation. A differentiation algorithm using two mapping functions was developed to convert the input data for a carcass's ROI pixels—the relative intensity of 580 nm and the ratio of intensities at 580 and 620 nm—into an output value indicating the carcass's probability of being systemically diseased in the ROI. Based on 63 sample images of systemically diseased chickens, it was determined that when a carcass's output value was higher than or equal to 0.65, the differentiation algorithm could identify the bird as being systemically diseased. The machine vision system was developed and evaluated for inspecting chickens on a commercial processing line operating at 140 bpm. During continuous multispectral inspection for one 8-h processing shift in a commercial processing plant, the machine vision system identified 0.11% (66 of 61,020) of chicken carcasses as systemically diseased. The rate of 0.11% was the same as that produced by the human inspectors working during the same shift. The fast imaging speed and effective image processing and differentiation algorithm that produced the high accuracy inspection results demonstrated that the

line-scan machine vision system was successfully developed and can be effectively used in a commercial chicken processing plant. Use of the system could produce significant benefits for increasing efficiency and reducing the effect of human error for the poultry processing industry.

References

1. USDA, *Pathogen Reduction: Hazard Analysis and Critical Control Point (HACCP) Systems*. Final Rule. Fed. Reg. 61: 28805–38855. (USDA, Washington, DC, 1996)
2. USDA, *Standard Operating Procedures for Notification and Protocol Submission of New Technologies* (USDA, Washington, DC, 2005)
3. W.R. Windham, D.P. Smith, B. Park, K.C. Lawrence, P.W. Feldner, Trans. ASABE **46**(6), 1733–1738 (2003)
4. C.-C. Yang, K. Chao, Y.-R. Chen, M.S. Kim, D.E. Chan, Biosys. Eng. **95**(4), 483–496 (2006). doi:10.1016/j.biosystemseng.2006.08.009
5. K. Chao, C.-C. Yang, Y.R. Chen, M.S. Kim, D.E. Chan, Poult. Sci. **86**(11), 2450–2460 (2007). doi:10.3382/ps.2006-00467
6. K.C. Lawrence, B. Park, W.R. Windham, C. Mao, Trans. ASABE **46**(2), 513–521 (2003)
7. M. Bjuggren, L. Krummenacher, L. Mattsson, Precis. Eng. **20**(1), 33–45 (1997). doi:10.1016/S0141-6359(97)00001-9
8. J.P. Connelly, S.W. Botchway, L. Kunz, D. Pattison, A.W. Parker, A.J. MacRobert, J. Photochem. Photobiol. A Chem. **142**(2–3), 169–175 (2001). doi:10.1016/S1010-6030(01)00511-1
9. L.K. Christensen, B.S. Bennedsen, R.N. Jorgensen, H. Nielsen, Biosys. Eng. **88**(1), 19–24 (2004). doi:10.1016/j.biosystemseng.2004.02.006